*Kovove Mater. 55 2017 89–96*
*DOI: 10.4149/km_2017_2_89*



# Microstructures of a pressure die cast Al-8.5%Si-3.5%Cu alloy

M. A. Barbes[1], M. J. Quintana[2], L. F. Verdeja[1], R. Gonzalez[2]*

[1] *School of Engineering of Mines, Energy and Materials of Oviedo, Universidad de Oviedo, Independencia 13, 33004, Oviedo, Spain*
[2] *Faculty of Engineering, Universidad Panamericana, Augusto Rodin 498, 03920, Mexico City, Mexico*

Received 12 January 2016, received in revised form 15 March 2016, accepted 22 April 2016

**Abstract**

Quantitative microstructural measurements of constituents of an Al-Si-Cu alloy, used to manufacture a part with thin sections by Pressure Die Casting (PDC), do not correspond to phase diagram calculations. A simulation of the liquid velocity when filling the mold was made in order to understand the relation between this parameter and pressure, cooling rate and the eutectic amount and morphology. Also, the microstructures of the same alloy solidified in a ceramic crucible (low cooling rate) and in a metal flask (high cooling rate) were compared to those obtained by PDC to analyze the role of pressure on the displacement of eutectic composition and formation of different eutectic morphologies. The amount of constituents varies with distance from the mold walls, producing higher or lower pressure zones, which may be estimated from the Al-Si phase diagram simulation at different pressures. As these pressures must be very high ($\sim$ 2 GPa), a possible explanation for the displacement of the eutectic point is the combination of high cooling rate of the manufacturing process, entrapment of gases during solidification and influence of the alloying elements.

K e y w o r d s: aluminum-silicon alloys, metallography, pressure die casting, cooling rate

## 1. Introduction

One of the most widely used aluminum die casting alloys is Al-8.5%Si-3.5%Cu (wt.%), with typical applications such as vacuum cleaners, floor polishers, and parts for automotive and electrical industries (motor frames, housings, etc.) [1]. Pressure Die Casting (PDC) of Al-Si-Cu alloys has been adopted by many casting industries in recent years as it allows very high production rates, near-net-shape geometries which require very few or null machining operations, complex designs with thin walls and low cost production associated with minimum waste and high repeatability of the process [2–4]. The design of the part and the manufacturing process takes advantage of the casting high pressure and the resulting high feeding rate in order to avoid turbulence, the formation of oxides and shrinkage defects on the final part [5]. Parts produced using this process may reach tensile stresses (UTS) of $\sim$ 240 MPa [2].

For an Al-8.5%Si-3.5%Cu alloy, the phases that would form with low cooling rates are a combination of binary (Al-Si) and ternary (Al-Si-$Al_2Cu$) eutectic phases and proeutectic $\alpha$ phase rich in Al [6] as shown in Fig. 1. The proeutectic $\alpha$ phase is observed as dendrites, while the eutectic morphologies are needles, polyhedra, lamellae and "chinese script" appearing in different shades of gray depending on the formation temperature and structure of the intermetallic compound [7, 8]. The size of proeutectic $\alpha$ grains, eutectic zones and Si particles determines mechanical properties, as higher strength and lower elongation may be reached with smaller dendrite spacing and compact Si particles [9]. However, the microstructure of this alloy produced by PDC shows constituents (proeutectic $\alpha$ and eutectic) in amounts that do not correspond to the ones indicated by the phase diagram. Furthermore, there are differences in the amount of constituents between the center and the surface zones of the mentioned tiles.

Microstructural characteristics of this type of Al-alloys are also influenced by the chemical composition and specific elements such as Fe and Mn [10]: both Fe and Mn increase melting and eutectic tem-

*Corresponding author: tel./fax: (52)55-54821600 ext. 5258; e-mail address: robglez@up.edu.mx

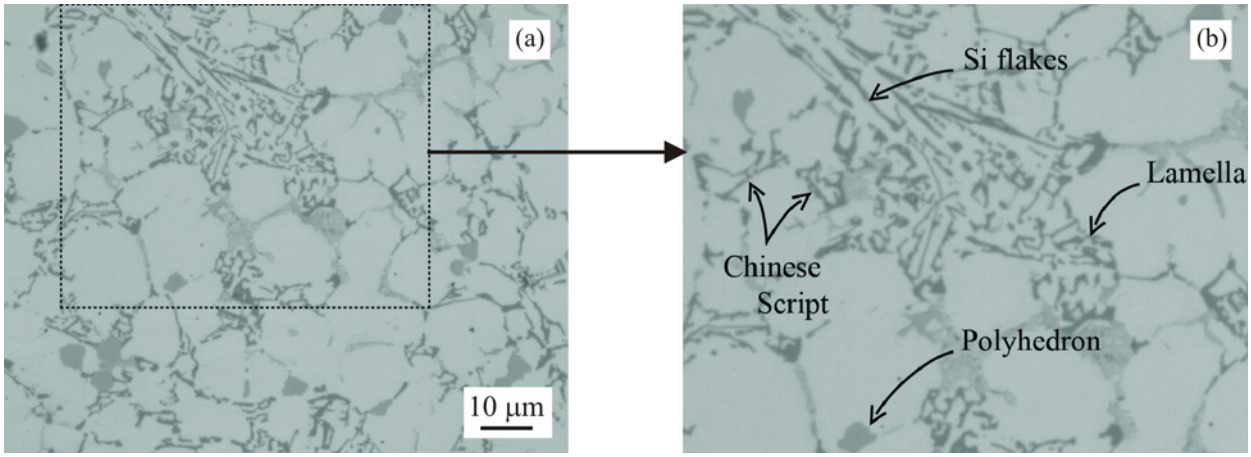


Fig. 1. The microstructure of the Al-8.5%Si-3.5%Cu alloy and enlargement showing different eutectic morphologies.

peratures and reduce the dendrite arm spacing, while Cu reduces these temperatures as well as a precipitate size, also avoiding agglomeration of Si particles. Fe/Mn ratio must be controlled in order to obtain a certain shape of Fe precipitates and reduce the length of needles.

The use of PDC, which is performed in very short periods of time and, consequently, using very high cooling rates, results in a microstructure with fine grain sizes and compact Si particles. Though the influence of cooling rates in the nucleation and final shape of $\alpha$ grains [11], as well as mathematical models used to simulate microstructure and displacement of the eutectic point caused by alloying elements [12, 13] have been reported, these works have not considered the effect of high pressure from both the die casting process and the gases trapped in the melt that are unable to escape from the solidifying parts.

Mechanical properties of parts produced by this method are also influenced by imperfections during solidification [14]. To reduce pores (most common imperfection), injection parameters, mold design and chemical composition (presence of $H_2$, oxides, borides, spinels, Li, Be, Ca, Na, Sr, and Mg) must be analyzed [15]. $H_2$ contained in the molten alloy will form entrapped bubbles as the solubility of this element diminishes with temperature [9].

## 2. Experimental procedure

The material analyzed in the present work is an Al-8.5%Si-3.5%Cu (with 1–1.3 % Fe, 0.5 % Mn, 0.1 % Mg, 3 % Zn) alloy used in PDC production of clean-room floor tiles. Samples from these tiles were obtained from different zones where thin sections must be filled and present adequate mechanical resistance (Fig. 2). Casting of this alloy in order to produce these parts is performed at 675 ℃ and pressure of 500 atm (50 MPa) in an injection equipment with horizontal chamber (*Bühler Evolution* and *Carat* equipment) in which the alloy is first prepared in an electric furnace, then placed in a waiting furnace in order to pour the injection quantities using a ladle with high diameter/depth ratio allowing degasification. The whole process of filling the injection chamber, injecting the molten alloy in the die, waiting for the alloy to cool down and solidify (using a water cooling system), opening the die and extracting the part, takes place in 30 s.

Also, the same alloy was used to cast specimens in both an alumina crucible and a metal flask to compare microstructures formed during solidification at low pressure and different cooling rates as the alumina crucible is highly refractory (long solidification time) and the metal flask is similar in thermal conductivity to the die used in PDC.

Standard metallographic techniques were used to section, grind and polish the samples in order to observe them in an optic microscope with a *Nikon Epiphot* equipment. The samples were observed as polished or, in some cases, etched with a solution of 10 g of NaOH, 5 g $K_3Fe(CN)_6$ in 60 ml $H_2O$ to darken the $Al_2Cu$ intermetallic.

To determine the volume fraction of phases other than $\alpha$, an *Omnimet* equipment connected to the *Nikon Epiphot* optic microscope was used with a 25-point mesh and semi-automatic detection. As indicated by Vander Voort [16], the mesh was used over images of the sample as many times as necessary to count more than 150 points lying in the phase being measured (eutectic), which resulted in an estimation error of $\sim 3$ % calculated through the standard deviation of each measurement and the distribution values for a 95 % confidence level. For each location analyzed, this procedure was made on three different tiles. The approximate Si content (wt.%) in the eutectic structure was calculated by the formula:

$$\%\mathrm{Si}_{\mathrm{eut}} = \frac{8.5 - 1.65}{V_{\mathrm{Veutectic}}} + 1.65, \qquad (1)$$

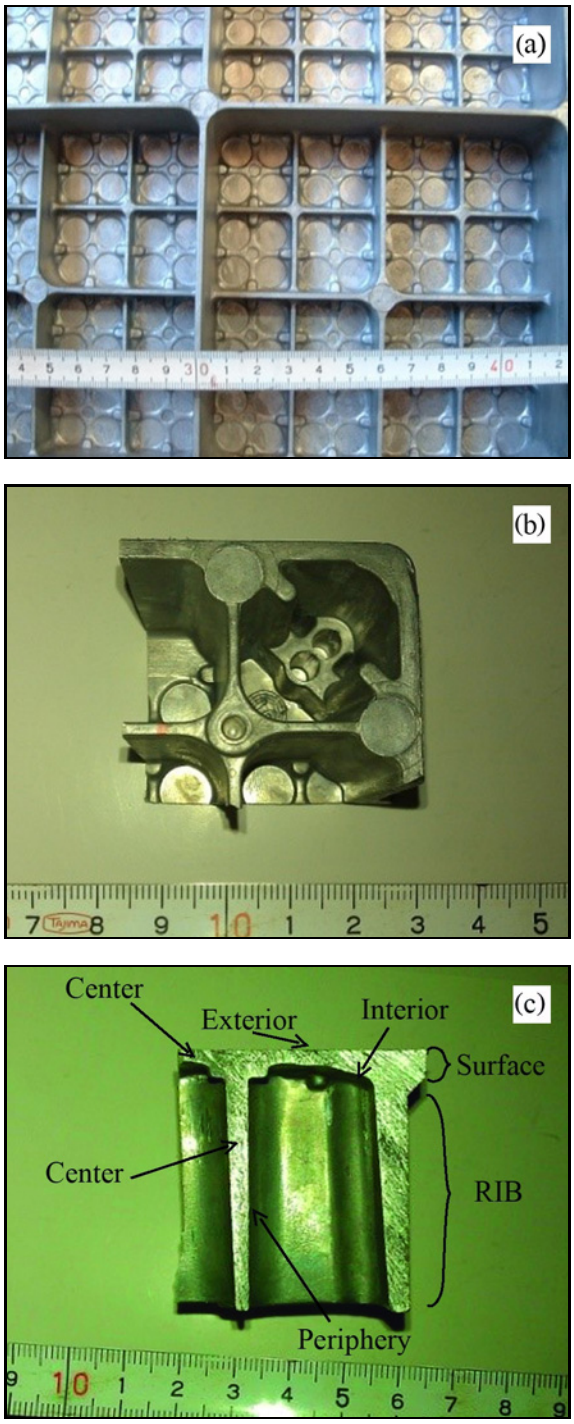


Fig. 2. Floor tile for technical applications (a), cornered sectioned for analysis (b) and a transverse section of the rib (c).

where $V_{\text{Veutectic}}$ is the volumetric fraction of eutectic measured, 8.5 is the mean content of Si in the alloy, and 1.65 is the maximum solubility of Si in Al. Considering $\rho_{\text{Al}} = 2{,}698.9\ \text{kg m}^{-3}$, $\rho_{\text{Si}} = 2{,}329\ \text{kg m}^{-3}$ and the phase diagram (weight composition), eutectic density results in $\sim 2{,}645.9\ \text{kg m}^{-3}$ (12.6 wt.% Si); this means that quantitative volumetric measurements are extremely similar to mass percentage calculations made on the phase diagram. It must also be considered that the addition of Cu usually decreases the solubility of Si in Al [17].

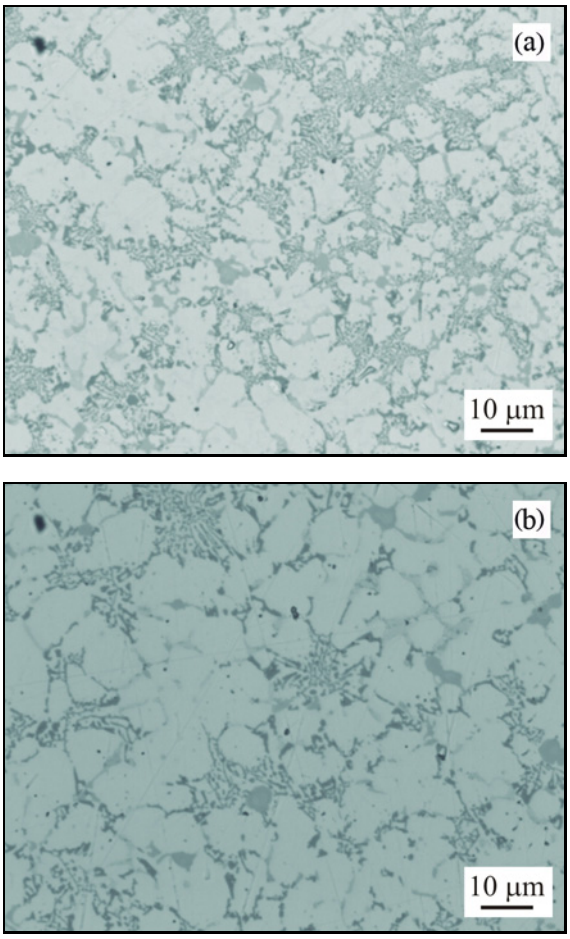


Fig. 3. Rib zone of the floor tile microstructure: periphery (a) and center (b) regions.

A finite element simulation using *ANSYS Workbench* of a 3D geometry similar to the ribs of the tile shown in Fig. 2c was made to simulate the different speeds of the melt inside the mold. The simulation considered a fluid velocity of $0.5\ \text{m s}^{-1}$ at the inlet face (left side of the 3D geometry) and liquid Al with a density of $2{,}700\ \text{kg m}^{-3}$ and a viscosity $\eta$ of 2.96 mPa s. Also, a viscous flow model of the *k-epsilon* type was selected to detect zones with laminar flow and zones with turbulences. Furthermore, *THERMOCALC* software was used to simulate the effect of pressure in the displacement of the eutectic composition and temperature values for an Al-8.5%Si alloy [18].

## 3. Results

Table 1 presents the mean values of the eutectic percentage measurements, as well as their error

Table 1. Quantitative metallography $V_v$ evaluation of measured phases, amount of Si in the eutectic (Eq. (1)) and morphology of eutectic phases

| | Eutectic (%) | $\alpha$ (%) | $Si_{eut}$ (%) | Eutectic morphology |
|---|---|---|---|---|
| Rib (periphery) | 44.4 ± 3.0 | 55.6 | 17.1 | Lamellae*, "chinese script", Si flakes, polyhedra |
| Rib (center) | 28.4 ± 2.2 | 71.6 | 25.8 | Lamellae*, "chinese script", Si flakes, polyhedra |
| Surface (exterior zone) | 40.2 ± 2.8 | 59.8 | 18.7 | Lamellae*, "chinese script", needles, polyhedra |
| Surface (center zone) | 28.8 ± 2.2 | 71.2 | 25.4 | Lamellae*, "chinese script", needles, polyhedra |
| Surface (interior zone) | 46.3 ± 3.0 | 53.7 | 16.4 | Lamellae*, "chinese script", needles, polyhedra |
| Metal flask casting | 48.0 ± 3.1 | 52.0 | 15.9 | Lamellae*, Si flakes, needle |
| Alumina crucible casting | 66.7 ± 3.4 | 33.3 | 11.92 | Lamellae*, "chinese script", needle |
| Phase diagram (theoretical) | ∼ 63 | ∼ 37 | 12.6 | |

*$Al_2Cu$ degenerated lamellae

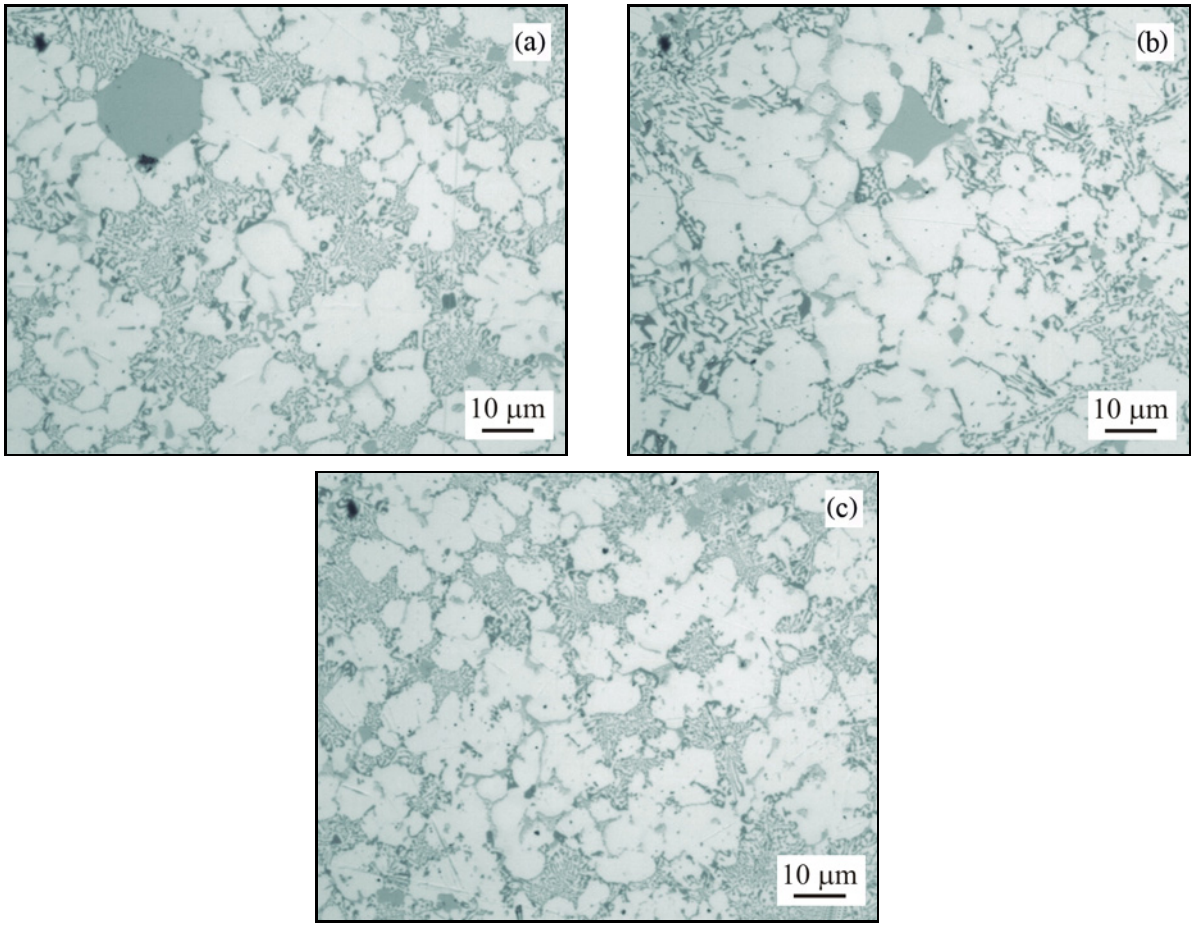


Fig. 4. Surface zone of the floor tile microstructures: interior (a), center (b) and exterior (c) regions.

estimation, made in different zones of the tile. Also, it shows the $\alpha$ and Si content estimation in each zone. As expected, optical microscopy of the different zones shows very low porosity, proeutectic grains ($\alpha$) and different types of eutectic distinguishable by their color, even without etchant. If the rib zone is analyzed (Fig. 3), differences between the periphery and the center are evident: the microstructure is formed by proeutectic $\alpha$ crystals and eutectic zones forming a continuous phase. Though the microstructures are similar, it is clear that a higher amount of $\alpha$ is present in the center region (Fig. 3b), as indicated in Table 1. In both figures the eutectic structure presents the same types of morphology: silicon flakes, polyhedra, $Al_2Cu$ lamellae (degenerated) and "chinese script", though $\alpha$ grains are slightly smaller at the periphery and lamellar spacing and length is also smaller at this location, indicating a higher cooling rate.

If the surface of the floor tile is analyzed, differences may also be found between the center, the ex-

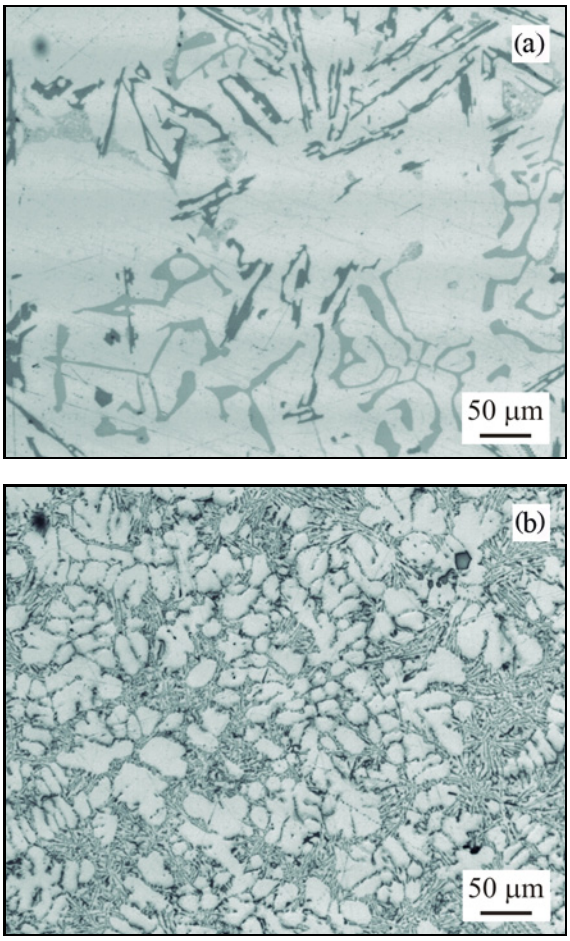


Fig. 5. Microstructure produced by casting in an alumina crucible (a) and metal flask (b).

terior and the interior of the floor (Fig. 4): again, the center zone presents a higher amount of $\alpha$, while the internal region has the lowest amount of this phase. Furthermore, eutectic phase includes "chinese script", needles, polyhedral, and $Al_2Cu$, and lamellar morphology does not seem to be present. A higher amount of both "chinese script" and $Al_2Cu$ can be found in the center zone (Fig. 4b), which may be related to a lower cooling rate [19, 20].

To measure the volume fractions of $\alpha$ and eutectic at atmospheric pressure conditions, the material was cast in a metal flask and in an alumina crucible. The resulting microstructure from the crucible (Fig. 5a) shows amounts ($\sim 67$ % eutectic and $\sim 33$ % $\alpha$) of phases very close to the ones expected from the phase diagram (Table 1), as solidification rate is very low and approximates invariant solidification conditions. Furthermore, the manufacturing process, and in this case, the high solidification rate caused by temperature loss through walls is better represented by casting in the metal flask (Fig. 5b): these two microstructures are very different as a higher cooling rate results in

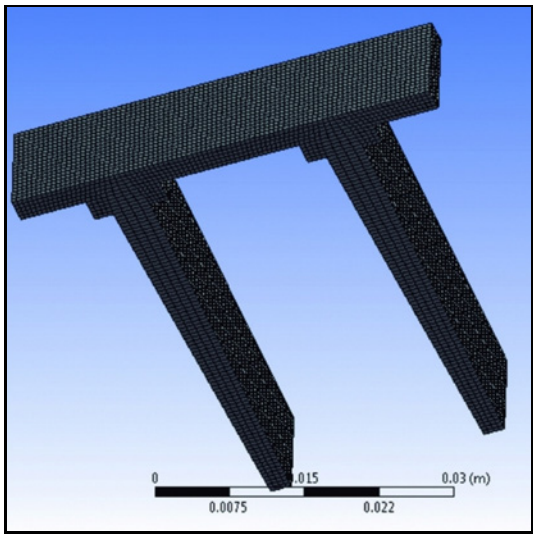


Fig. 6. Profile of the floor tile, similar to that of Fig. 2c, in ANSYS.

smaller $\alpha$ grains surrounded by eutectic (short needles and lamellae), while a longer solidification period induces very large $\alpha$ grains surrounded by eutectic (long needles in a darker color and large "chinese script" in a lighter color). The size of the "chinese script" phase formed in the alumina crucible is considerably larger in comparison to the ones produced by pressure casting.

## 4. Discussion

For an Al-alloy with 8.5 % Si, the lever rule analysis of the phase diagram results in a 63 % eutectic phase and 37 % $\alpha$ (mass percentage calculations are very similar to the volumetric ones), which are very far from the quantitative measurements (Table 1) of the microstructures of Figs. 3, 4 and 5. Suarez-Peña et al. [21] have reported the same anomaly (a large amount of proeutectic $\alpha$ phase) in eutectic or quasi-eutectic Al-Si alloys produced by PDC in the same industrial facility and using identical equipment. Though slight differences could be explained by major elements segregation, these microstructures can be the result of pressure and the displacement of the eutectic temperature and eutectic composition [21]: variations in the $V_V$ of $\alpha$-phase as high as 37–46 % can be found in hypoeutectic Al-Si compositions.

To understand the behavior of the liquid Al alloy during the filling of the die, an *ANSYS Fluent* (15.0 version) finite element simulation was performed in a geometry closely resembling the one shown in Fig. 2, and using a total of 24,000 elements (Fig. 6). The simulation included turbulent flow considerations as a laminar behavior cannot be expected when thin closed

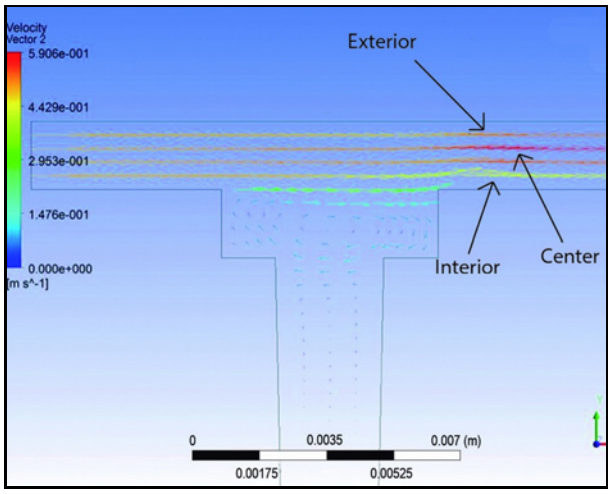


Fig. 7. The fluid velocity of the liquid Al through the tile profile.

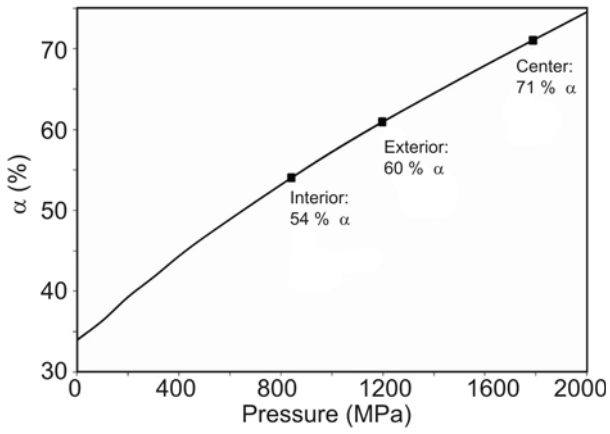


Fig. 9. Tendency curve for $\alpha$ phase amount as a function of pressure according to [22] and measurements at the surface zone.

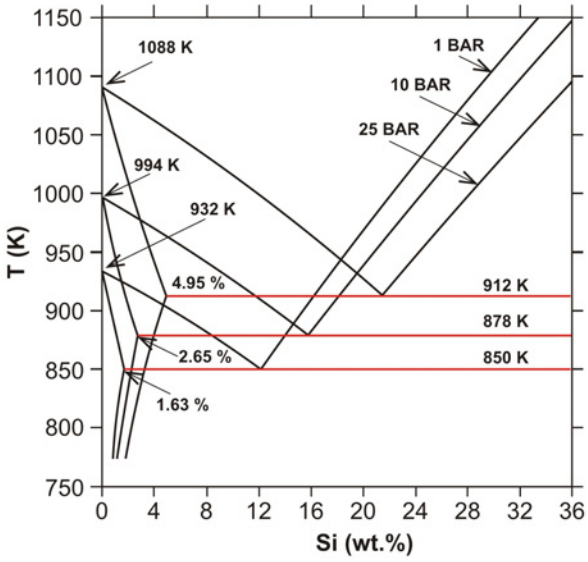


Fig. 8. Pressure influence in THERMOCALC phase diagram simulation for the Al-Si system.

spaces are to be filled with liquid during casting. An almost perfect laminar flow is observed at the tile surface (Fig. 7), where the fluid behaves in the following way: velocity is highest at the center zone, the wall of the exterior of the tile has a lower velocity though still higher than the one near the wall of the interior of the tile.

In this type of casting, three processes occur in a very quick succession: filling the mold, hydrostatic pressure, and cooling of the part. The $V_V$ amounts of $\alpha$ and eutectic at the different zones of the part can be explained by the velocity of the fluid inside the mold (Fig. 7): the slower zones will cause the material to be in the first stages of the solidification process resulting in different microstructures compared to zones with higher speeds [3].

These variations in the solidification rate can produce changes in pressure which also result in modifications to the amount of constituents in the microstructure since the pressure difference causes the eutectic point to move towards higher Si content as well as higher temperatures, meaning that the tile zones will each have specific eutectic parameters [22].

Other works, using FEM, have also shown that metal injection molding with high pressure will result in pressure differences between zones of the die [23] similar to the ones shown in Fig. 4. These pressure variations may change grain size and distribution [24] and also a higher amount of $\alpha$ phase in zones farther from the die walls [3]. To better understand the data presented in Table 1, a thermodynamic phase diagram simulation was made using *THERMOCALC*. As this software does not include information to change pressure as a variable in the system in its database, the following formulas were considered:

– for $\alpha$ phase: $\mathrm{d}G_\alpha = -S_\alpha \mathrm{d}T + V_\alpha \mathrm{d}P$,
– for pure Si: $\mathrm{d}G_{\mathrm{Si}} = -S_{\mathrm{Si}} \mathrm{d}T + V_{\mathrm{Si}} \mathrm{d}P$,
– for liquid phase: $\mathrm{d}G_{\mathrm{L}} = -S_{\mathrm{L}} \mathrm{d}T + V_{\mathrm{L}} \mathrm{d}P$,

where $G$ is free energy, $S$ is enthalpy, $T$ is temperature, $V$ is volume of the phase, and $P$ is the pressure of the system. The total value of the $V\mathrm{d}P$ term for each of the pressures analyzed was introduced into the database in order to simulate the phase diagram. The result of the simulation is presented in Fig. 8, which is similar to data presented by other authors [3].

From data presented by Sobczak et al. [22], as shown in Fig. 9, the pressures required to obtain the amount of constituents at the surface zone of the tiles would be: $\sim 1.8$ GPa at the center, $\sim 1.15$ GPa at the exterior and $\sim 843$ MPa at the interior, which are orders of magnitude higher than the ones expected from

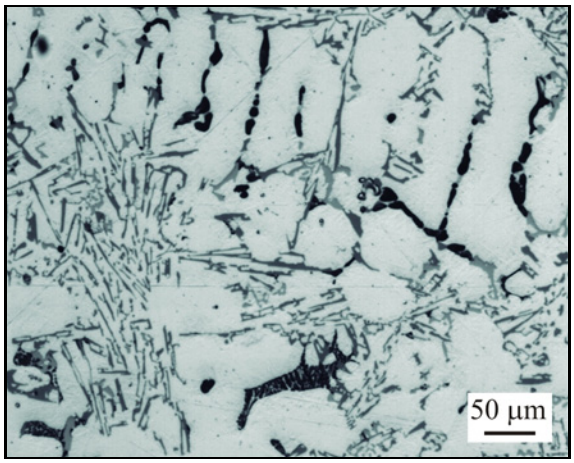


Fig. 10. Microstructure produced by casting in a metal flask etched with NaOH and $K_3Fe(CN)_6$ showing $Al_2Cu$ as the darker phase.

the PDC (only 50 MPa injection pressure).

Another explanation of pressure variations at different zones of the tile is that during the solidification process, the alloy expels gases which are dissolved in the liquid metal, as cooling takes place. These gases are usually observed as pores in final parts: the gas that the metal rejects during solidification travels towards the surface of the part and into the atmosphere. Thus, in the tile, the gas will move from low-temperature towards high-temperature zones in which solubility is higher. As those zones of the part with high temperature become saturated with $H_2$ (and even more as they suffer their own decrease in temperature) and, due to the lack of bubble-forming agents, the $H_2$ will rapidly move through the part. Such extreme conditions of cooling and exterior pressure will prevent the bubble from growing during solidification, and all the gas will stay entrapped in the liquid [25].

An analysis of Figs. 4 and 5b shows that the morphology of the proeutectic $\alpha$ phase is not affected by pressure, as in both cases, injected parts in steel molds or cooled in a metal flask present dendritic shape. On the other hand, Fig. 5a shows needle-shaped eutectic when the material cools in an alumina crucible, as phases such as Si and "chinese script" are allowed to grow and coalesce as liquid remains during much longer periods of time. Thusly, eutectic morphology and size seem to be affected only by cooling rate (and not pressure) which is a factor that changes with the refractoriness of the mold and/or the heat removal capacity of the cooling system.

Another evidence of the different cooling rates at the zones analyzed for the part is the presence of more than one morphology in the eutectic regions (Table 1). As an example, lamellae seem to appear at zones rapidly cooled, at the rib (Fig. 3) and at the metal flask (Fig. 5b). Also, increasing cooling rate and the use of pressure is connected to the formation of polyhedra as the alumina crucible and the metal flask do not present this morphology.

Furthermore, the eutectic morphologies observed are evidence of solidification phenomena of both binary (Al-Si) and ternary (Al-Si-Cu) reactions occurring at very different temperatures [26, 27]. Figure 10 shows the metal flask microstructure etched with 10 g of NaOH, 5 g $K_3Fe(CN)_6$ in 60 ml $H_2O$ in order to darken the $Al_2Cu$ intermetallic, which has a morphology evidently different from the other eutectics, confirming that it is formed at a lower temperature [6].

As eutectic phases are formed at more than one temperature depending on the cooling rate of each zone, this could also be an explanation for the variations in proportions of both proeutectic $\alpha$ phase and eutectics, as well as the different morphologies presented at each location.

If the dendrite arm spacing is considered as an indication of the cooling rate at different zones, Cho and Kim [28] measured an alloy with a composition very similar to the one analyzed in this work during PDC and estimated cooling rates as a function of this parameter. Comparison between the dendrites of the periphery and the center of the rib (Fig. 3) indicates that the center zone ($\sim 40\,^{\circ}\mathrm{C\,s^{-1}}$) cools slower than the periphery ($\sim 60\,^{\circ}\mathrm{C\,s^{-1}}$) as it is in contact with the mold wall. Also, the dendrites of the rib periphery and the surface interior (Fig. 4a) have approximately the same arm spacing ($\sim 60\,^{\circ}\mathrm{C\,s^{-1}}$). The surface exterior (Fig. 4c) shows the highest cooling rate ($\sim 70\,^{\circ}\mathrm{C\,s^{-1}}$) as it is a flat geometry in contact with the mold. If Fig. 9 is considered, where the interior has a lower amount of $\alpha$ phase than the exterior, it can be assumed that the cooling rate is not directly related to the amount of proeutectic $\alpha$ phase, even though the cooling rate of the exterior is higher.

## 5. Conclusions

High pressure conditions during injection, and very high cooling rates (all the steps of the injection process are performed in 30 s) may explain the microstructural differences of the material cooled in the alumina crucible, the one cooled in the metal flask and the various locations of the tile analyzed. The large amounts of $\alpha$ phase in the PDC parts cannot be satisfactorily explained only by the effect of bulk material segregation but by the changes in solidification rates at the various locations of the mold/part resulting in lamellae, needles, "chinese script," polyhedra, and $Al_2Cu$ present in different quantities.

Though injected parts show a large amount of $\alpha$ phase, percentage variations between the center, the interior, and the exterior regions are still evident: Center has $\sim 15$ % more $\alpha$ as its cooling rate is lower

than in zones in contact with the mold during solidification. Differences in the velocity of the fluid through the mold added to the hydrostatic pressure of the casting process could result in microstructural changes at various zones of the part as each one has a particular eutectic composition and temperature.

## Acknowledgements

The authors wish to thank Jose Garcia of the Metallurgy Department at Oviedo University for sample preparation and microstructural features analysis, Bertha Mendieta for figure preparations as well as the Research Assistant Fund both at the Faculty of Engineering of Universidad Panamericana.

## References

[1] Kearney, A. L. (Ed.): Metals Handbook. Properties of Cast Aluminum Alloys. Volume 2. Metals Park, American Society for Metals 1990.
[2] Warmuzek, M. (Ed.): Aluminum-Silicon Casting Alloys: Atlas of Microfractographs. Introduction to Aluminum-Silicon Casting Alloys. Metals Park, ASM International 2004.
[3] Ji, S., Wang, Y., Watson, D., Fan, Z.: Metall. Mater. Trans. A, *44*, 2013, p. 3185. doi:10.1007/s11661-013-1663-5
[4] Asensio, J., Suárez-Peña, B.: Mater. Charact., *56*, 2006, p. 169. doi:10.1016/j.matchar.2005.10.016
[5] Casari, D., Merlin, M., Garagnani, G. L.: Metall. Sci. Tech., *30*, 2012, p. 12.
[6] Raghavan, V.: J. Phase Equilib. Diff., *28*, 2007, p. 180. doi:10.1007/s11669-007-9024-y
[7] Kevorkijan, V., Skapin, S. D.: Metall. Mater. Eng., *16*, 2010, p. 47.
[8] Warmuzek, M., Ratuszek, W., Sek-Sas, G.: Mater. Charact., *54*, 2005, p. 31. doi:10.1016/j.matchar.2004.10.001
[9] Grosselle, F., Timelli, G., Bonollo, F., Molina, R.: Metall. Sci. Technol., *27*, 2009, p. 2.
[10] Gowri, S., Samuel, F. H.: Metall. Mater. Trans. A, *25*, 1994, p. 437. doi:10.1007/BF02647989
[11] Krupinski, M., Labisz, K., Dobrzanski, L. A.: J. Achievements Mater. Manuf. Eng., *34*, 2009, p. 47.
[12] Zhu, M. F., Hong, C. P.: Metall. Mater. Trans. A, *35*, 2004, p. 1555. doi:10.1007/s11661-004-0262-x
[13] Djurdjevic, M. B., Vicario, I.: Rev. Metal. Madrid, *49*, 2013, p. 340. doi:10.3989/revmetalm.1238
[14] Colás, R., Rodríguez, J., Valtierra, S.: Int. J. Cast Metal. Res., *17*, 2004, p. 332. doi:10.1179/136404604225022739
[15] Pietrowski, S., Pisarek, B., Wladysiak, R.: Arch. Foundry Eng., *11*, 2011, p. 109.
[16] Vander Voort, G. F.: Metallography Principles and Practice. Materials Park, ASM International 2007.
[17] Plaza, D., Pero-Sanz, J. A., Verdeja, J. I.: Rev. Minas., *11–12*, 1995, p. 99.
[18] Chernov, D. B., Schinyaev, A. Ya.: Nauka, 1974, p. 80.
[19] Jun, J. H.: Mater. Trans., *53*, 2012, p. 2064. doi:10.2320/matertrans.M2012255
[20] Tang, S., Zhou, J., Tian, C., Yang, Y.: Trans. Nonferrous Met. Soc. China, *21*, 2011, p. 1932. doi:10.1016/S1003-6326(11)60952-7
[21] Suárez Peña, B., Asensio, J., Verdeja, J. I., Pero-Sanz, J. A.: Rev. Metal Madrid, *43*, 2007, p. 310.
[22] Sobczak, J. J., Drenchev, L., Asthana, R.: Int. J. Cast Met. Res., *25*, 2012, p. 1. doi:10.1179/1743133611Y.0000000016
[23] Berginc, B., Brezocnik, M., Kampus, Z., Sustarsic, B.: Mater. Technol., *43*, 2009, p. 43.
[24] Raji, A., Khan, R. H.: Au J. Tech., *9*, 2006, p. 229.
[25] Chen, Y. J.: Mater. Trans., *50*, 2009, p. 2308. doi:10.2320/matertrans.M2009179
[26] Ponweiser, N., Richter, K. W.: J. Alloy Compd., *512*, 2012, p. 252. doi:10.1016/j.jallcom.2012.04.096
[27] Ashtari, P., Tezuka, H., Sato, T.: Mater. Trans., *44*, 2003, p. 2611.
[28] Cho, J. I., Kim, C. W.: Int. J. Metalcasting, *8*, 2014, p. 49. doi:10.1007/BF03355571